ChemComm

COMMUNICATION

View Article Online
View Journal | View Issue

Cite this: *Chem. Commun.*, 2015, **51**, 10831

Received 12th April 2015,
Accepted 20th May 2015

DOI: 10.1039/c5cc03028e

www.rsc.org/chemcomm

A porphyrin photosensitized metal–organic framework for cancer cell apoptosis and caspase responsive theranostics†

Lei Zhang, Jianping Lei,* Fengjiao Ma, Pinghua Ling, Jintong Liu and Huangxian Ju*

A photosensitized and caspase-responsive multifunctional nanoprobe was designed by assembling a porphyrin, a folate targeting-motif and a dye-labelled peptide in a metal–organic framework (MOF) cage, which significantly increases the singlet oxygen quantum yield of porphyrin by 6.2 times, and achieves high efficient cancer therapy and *in situ* therapeutic monitoring with caspase-3 activation. The integration of theranostic functions in a single nanocarrier holds great promise in precision cancer diagnosis and treatment.

Porphyrin derivatives are the most widely applied photosensitizers in photodynamic therapy against a variety of cancers because of their high efficiency in light harvesting and tunable structure.[1] However, the hydrophobicity of many porphyrins results in their aggregation and insufficient tumor localization.[2] To improve the therapeutic efficacy, a well-performing nanocarrier is usually needed to selectively deliver these porphyrin derivatives to tumor targets.[3] Recently, metal–organic frameworks (MOFs), an emerging class of porous materials, have captured prevailing research interest in drug delivery, biosensing and cancer therapy,[4] due to their unprecedentedly large surface area, unique inner porosity and flexible structures.[5] In particular, some porphyrin-based MOFs, which show interesting peroxidase activity, have been used in mimetic catalysis.[6] More recently, the Hf^{4+}-porphyrin based MOF has been designed as a highly effective photosensitizer in therapy for treatment of resistant head and neck cancer.[7] To enhance the therapeutic efficacy and to avoid under- or over-treatment, the integration of theranostic functions in a single nanocarrier is urgently needed in the therapeutic monitoring of cancer for precision treatment.

Photosensitizers that can be activated with intrinsic fluorescence can be developed for therapy and imaging of cancer cells with respect to an enzyme expression such as caspase.[8] Caspases are a family of cysteine–aspartic proteases that are activated only during cell apoptosis,[9] and have been used as sensors for apoptosis imaging and evaluating therapeutic responses.[10] Coupling the apoptosis-inducing capability of photosensitizers with the subsequent caspase activation,[11] the integration of theranostic functions can be achieved in a single nanocarrier. However, the conventional photosensitizers are significantly affected by photobleaching. In view of the structural diversity, tunability and capacity for modification of MOFs to protect both photosensitivity and fluorescence,[12] a multifunctional nanoprobe was designed here for efficient cancer-cell-specific therapy and monitoring the therapeutic effectiveness *via* caspase-dependent apoptosis imaging (Scheme 1).

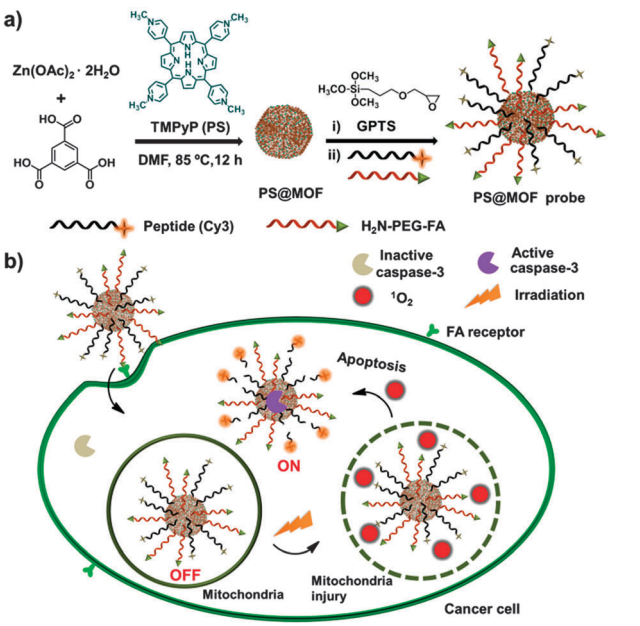

Scheme 1 Schematic representation of (a) the PS@MOF probe preparation and (b) FA receptor-targeted delivery of the multifunctional PS@MOF probe for cancer cell apoptosis and theranostic with caspase-3 activation.

State Key Laboratory of Analytical Chemistry for Life Science, Collaborative Innovation Center of Chemistry for Life Sciences, School of Chemistry and Chemical Engineering, Nanjing University, Nanjing 210093, P. R. China.
E-mail: jpl@nju.edu.cn, hxju@nju.edu.cn; Fax: +86 25 83593593;
Tel: +86 25 83593593

† Electronic supplementary information (ESI) available: Experimental details and additional figures. See DOI: 10.1039/c5cc03028e

The porphyrin derivative, tetrakis(1-methylpyridinium-4-yl)-porphyrin (TMPyP), as the photosensitizer (PS), could be incorporated into the cage of a variant MOF by one-pot synthesis to form the PS@MOF. The transmission electron microscopy (TEM) image of the PS@MOF showed a twisted boracite morphology (Fig. 1a). The nitrogen adsorption–desorption isotherm of the PS@MOF gave a micropore size of around 1.50 nm (Fig. S1, ESI†), closely matching the reported porphyrin-encapsulated variant HKUST-1.[13] The PS@MOF displayed an X-ray diffraction pattern obviously different from that of the TMPyP-free MOF (Fig. S2, ESI†), indicating the existence of TMPyP in the MOF. The encapsulation was proved by the unaltered fluorescence anisotropy curves of TMPyP, which usually changed with the direct interactions between the fluorophores and nanoparticles (Fig. S3, ESI†).[14] The hydrophobic nature of the MOF cavity led to an obvious bathochromic-shift of the Soret-band of TMPyP in the MOF (Fig. 1b).[15] Although the strong absorption of TMPyP in the MOF occurred at 442 nm, its NIR characteristic absorption at around 667 nm shifted from 645 nm upon encapsulation in the MOF (inset in Fig. 1b) was used as the irradiation wavelength for photodynamic therapy due to its desirable application in living cells. By measuring the absorbance at 420 nm, a loading efficiency of TMPyP in the MOF was estimated to be 32.8% (Fig. S4, ESI†). Dynamic light scattering (DLS) of PS@MOF showed an average nanosized hydrodynamic diameter (Fig. 1c), which was beneficial to intracellular assays.

In order to assemble the Cy3-labelled caspase-3 substrate peptide and H_2N–PEG–folate (FA) on PS@MOF, the surface was firstly functionalized with (3-glycidyloxypropyl)trimethoxysilane (GPTS) to obtain epoxy-terminated PS@MOF–GPTS, which was characterized by a broad band at approximately 1000 cm^{-1} on its infrared (IR) spectrum due to the asymmetric stretching vibration of the Si–O group (Fig. 1d).[16] With the typical reaction of epoxy and amino groups, the peptide and the H_2N–PEG–FA functionalized PS@MOF nanoprobe were found to show a new characteristic absorption at around 280 nm and 529 nm (Fig. 1e), which were assigned to FA and Cy3 labeled to the peptide, respectively. The surface of the PS@MOF nanoprobe showed a more negative potential after being modified with the electronegative peptide (Fig. 1f), indicating a better dispersibility of the nanoprobe in water. The coupling amount of the peptide was determined to be 37.1 mg g^{-1} (Fig. S5, ESI†). The nanoprobe could maintain a high stability for 30 h in PBS (Fig. S6, ESI†), which was favorable for the internalization of the nanoprobe by cancer cells *via* a folate receptor (FR)-mediated endocytosis.

The efficient release of singlet oxygen ($^1O_2$) is a major challenge for photodynamic therapy (PDT) against cancer cells. The $^1O_2$ production under laser irradiation was demonstrated with 1,3-diphenylisobenzofuran (DPBF) as an $^1O_2$ indicator, which could decrease the optical density (OD) at 418 nm upon reaction with $^1O_2$.[17] After individually exposing TMPyP, MOF and PS@MOF solution to a 660 nm irradiation for 210 s, PS@MOF solution showed a much greater change in OD than free TMPyP, while the MOF in the absence of TMPyP exhibited little variation (Fig. 2a). The surface functionalization of the PS@MOF with the peptide and FA did not affect the $^1O_2$ generation. Furthermore, the $^1O_2$ generation dynamic was fast, which trended to the maximum consumption of the indicator at 90 s (Fig. 2a and b). Using methylene blue (MB) as a standard, the $^1O_2$ quantum yield (Φ_Δ) could be calculated. It increased from 0.10 ± 0.02 for TMPyP to 0.61 ± 0.05 for the PS@MOF under a 660 nm irradiation, indicating a 6.2 times improvement of the photosensitivity of TMPyP by the MOF structure.

Considering that the property of excited states is the key factor in the $^1O_2$ generation, a simplified energy level diagram was illustrated in Fig. 2c. The energy level gap of S_1–S_0 for the PS@MOF was consistent with TMPyP, derived from the unshifted fluorescence emission wavelength of TMPyP (Fig. S7a, ESI†), while the blue-shifted phosphorescent emission of the PS@MOF showed a widened difference of T_1–S_0 (Fig. S7b, ESI†). The narrowed S_1–T_1 gap boosted the intersystem crossing from S_1 to T_1, and the longer

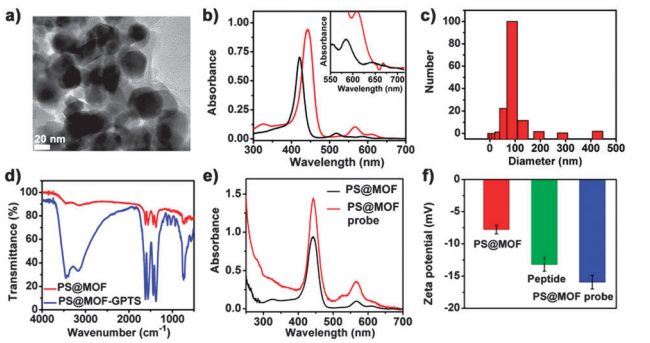

Fig. 1 (a) TEM image of PS@MOF. (b) UV-Vis absorption spectra of TMPyP (black) and PS@MOF (red). Inset: an enlarged view of UV-Vis spectrum of TMPyP and PS@MOF at 550–715 nm. (c) DLS assay of PS@MOF. (d) IR spectra of PS@MOF and GPTS-functionalized PS@MOF. (e) UV-Vis absorption spectra of PS@MOF and PS@MOF nanoprobe. (f) Zeta potential of PS@MOF, caspase-specific peptide and PS@MOF nanoprobe.

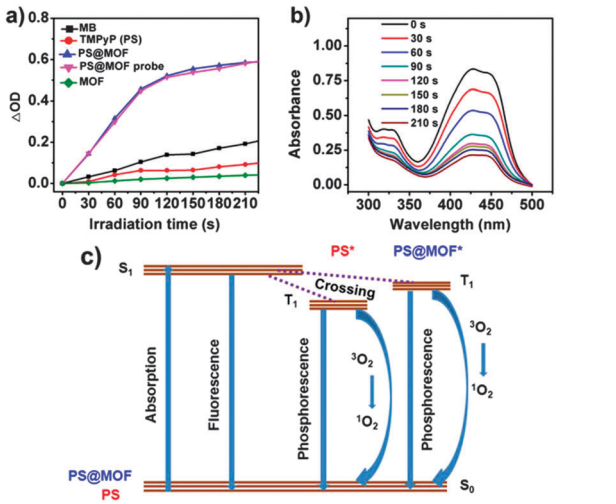

Fig. 2 (a) Plots of change in OD of DPBF (60 μM) in TMPyP (2.0 μM), MOF (1.0 mg mL^{-1}), PS@MOF (2.0 μM, PS equiv.), PS@MOF nanoprobe (2.0 μM, PS equiv.) solution or MB (2.0 μM) as the standard at 418 nm *vs.* irradiation time. (b) Monitoring of $^1O_2$ generated from the PS@MOF nanoprobe upon irradiation using DPBF as $^1O_2$ indicator. (c) Modified Jablonski diagram illustrating the process of photosensitized $^1O_2$ production. S_0, singlet ground state; S_1, singlet excited state; T_1, triplet excited state.

average lifetime (τ_P) of T_1 also verified the more excited state of PS@MOF in T_1 (Table S1, ESI†). However, the enhanced intersystem crossing did not necessarily result in the energy transmission from the excited PS@MOF toward $^3O_2$ to generate more $^1O_2$, since a competitive relationship existed between $^1O_2$ generation and phosphorescence emission when electrons transfer from T_1 to S_0. The phosphorescence quantum yield (Φ_P) was also measured in Table S1 (ESI†). After being encapsulated in the MOF, TMPyP showed a Φ_P of only ~34% that in free state, indicating that more energy of the excited PS@MOF was transferred to $^3O_2$ to generate $^1O_2$. The high light-harvesting of the PS@MOF platform could be attributed to the exact structural match between TMPyP and the MOF, which inhibited the free vibration and rotation of the four pyridyl arms, leading to a high fluorescence quantum yield (Φ_F) and short fluorescence lifetime (τ_F) (Table S1, ESI†).[12,13,18]

To test the validity of the PS@MOF nanoprobe to detect caspase activity, *in vitro* enzymatic assays were performed (Fig. S8, ESI†). The probe fluorescence was initially quenched *via* an electron transfer from Cy3 to the MOF (Fig. S9, ESI†).[19] At the optimized reaction time of 60 min, the fluorescence intensity linearly increased with the enhanced concentration of caspase-3 to cleave the substrate peptide on the probe, leading to a fluorescence method for the detection of caspase-3 activity. The cleavage reaction showed good specificity to caspase against other proteins (Fig. S8, ESI†), which may interfere with the detection of caspase in living cells. The *in vitro* experiments indicated the great potential of the PS@MOF nanoprobe in intracellular caspase activity study.

After an 8 h incubation with human cervical carcinoma (HeLa) cells based on the FR-targeted endocytosis,[20] the PS@MOF nanoprobe was observed to be distributed in the mitochondria (Fig. S10a–c, ESI†). Little fluorescent spots were observed in the well grown cells before laser irradiation, indicating that caspase was inactive before cell apoptosis. Upon 660 nm laser irradiation for 15 min, cell apoptosis was encouraged by the PS@MOF-mediated $^1O_2$, and Cy3 fluorescence of the nanoprobe was lighted up (Fig. 3a). To clarify the production of reactive oxygen species (ROS) during the irradiation, the nanoprobe-treated HeLa cells were stained with DCFH-DA, a nonfluorescent ROS probe, which was turned into a highly fluorescent product upon oxidation by ROS (Fig. S11, ESI†). Meanwhile, vitamin C as an ROS scavenger efficiently reduced the fluorescence of the ROS probe. For different postirradiation times, the nanoprobe fluorescence gradually increased with the deepened degree of cell apoptosis (Fig. 3a), indicating that caspase-3 was activated during cell apoptosis and the caspase-activable fluorescence imaging was an effective tool for monitoring the therapeutic efficacy.

The lighted HeLa cells were co-stained with a mitochondrial dye, which showed that the nanoprobe diffused from mitochondrial to cytoplasm after the injury of mitochondria with laser irradiation (Fig. S10c and d, ESI†). The mitochondrial injury was confirmed by Rhodamine 123 staining,[21] which is readily sequestered by living mitochondria in cells undergoing apoptosis, manifesting the mitochondrial-pathway apoptosis (Fig. S12, ESI†). In addition, unlike HeLa malignant cells, the nanoprobe-treated human epidermal (HaCat) normal cells, due to the low-level expression of FR, did not show observable fluorescence before and after laser irradiation in confocal imaging and flow cytometric analysis (Fig. S13 and S14, ESI†).

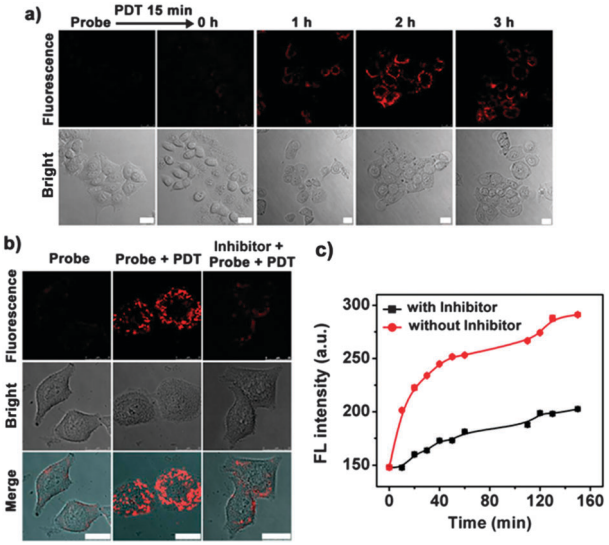

Fig. 3 (a) Confocal imaging monitoring of fluorescence and bright-field of PS@MOF nanoprobe-incubated HeLa cells at different postirradiation times upon irradiation with a 660 nm-laser at 100 mW cm^{-2} for 15 min. Scale bar, 25 μm. (b) Confocal fluorescence imaging of HeLa cells pre-incubated with/without caspase-3 inhibitor during PS@MOF nanoprobe-mediated PDT. Scale bars, 25 μm. (c) Time-dependent fluorescence response of the PS@MOF nanoprobe to cell lysate treated with PS@MOF–FA for 8 h and laser irradiation for 15 min.

The specifically caspase-activable fluorescence imaging was confirmed with caspase inhibitor treatment. After caspase-3 inhibitor-pretreated HeLa cells were incubated with the PS@MOF nanoprobe and exposed to laser irradiation, the fluorescence was greatly reduced in comparison with that of inhibitor-untreated cells (Fig. 3b). For further verifying the caspase activation during the therapy, a peptide-free probe was synthesized, named as PS@MOF-FA. After incubation with PS@MOF–FA for 8 h and treatment with irradiation for 15 min, HeLa cells were collected in lysis buffer after 2 h postirradiation. The cell lysate was then incubated with the PS@MOF nanoprobe for fluorescence measurements in a time-dependent manner. A tendency for rapidly increased fluorescence intensity was observed in the absence of caspase inhibitor (Fig. 3c), suggesting that caspase-3 was indeed activated in an apoptotic process. Moreover, the caspase-activable fluorescence during cell apoptosis was demonstrated by the TUNEL assay using the additional apoptotic kit (Fig. S15, ESI†). When HeLa cells were treated with the PS@MOF nanoprobe-mediated PDT, the cells showed strong Cy3 fluorescence originating from caspase dependent activation and cleavage, which could be used to monitor therapeutic efficacy.

The nanoprobe-caused phototoxicity and therapeutic effectiveness against cancer cells were also evaluated and compared with a conventional photosensitizer, chlorin e6 (Ce6). At each photosensitizer concentration, the cytotoxicity of the correspondingly treated cells was examined using a standard MTT assay (Fig. 4a). Before laser irradiation, these photosensitizers were little cytotoxic. An 8 h incubation with the PS@MOF nanoprobe could maintain about 95% cell viability at the concentrations of 0.5–3.5 μM (PS equiv.), demonstrating low dark-toxicity of the PS@MOF nanoprobe. To some extent, the PS@MOF nanoprobe was more biocompatible

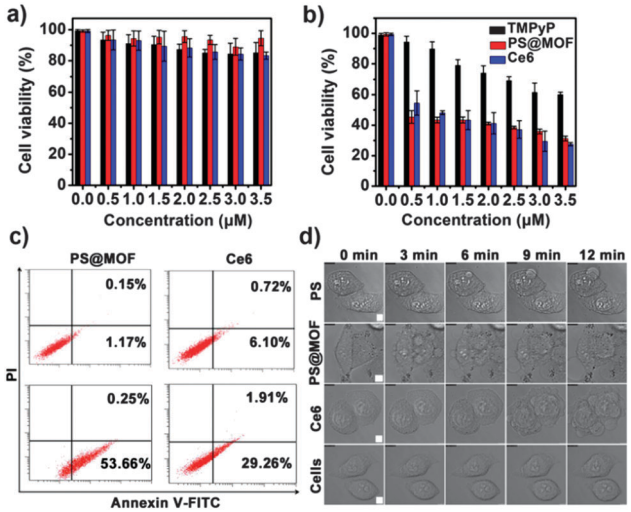

Fig. 4 MTT assays for HeLa cells incubated with PDT agents of different concentrations in the absence (a) and the presence (b) of laser irradiation. (c) Flow cytometric analysis of HeLa cells incubated with the PS@MOF nanoprobe (0.5 μM, PS equiv.) and Ce6 (0.5 μM) for 8 h before (top) and after (down) laser irradiation for 15 min using apoptosis kit with the dual fluorescence of annexin V-FITC/PI. (d) Monitoring of the morphology change of HeLa cells treated with different PDT agents (1.0 μM) for 8 h and then laser irradiation at 100 mW cm^{-2} for different time. Scale bars, 7.5 μm.

than free TMPyP and Ce6, indicating that the MOF could protect TMPyP from biotoxicity. Under a 15 min irradiation with a 100 mW cm^{-2} dose, all these reagents exhibited obvious phototoxicity (Fig. 4b). The cell viability of the PS@MOF probe- and Ce6-treated HeLa cells was much lower than those treated with TMPyP under the same conditions. Meanwhile, the PS@MOF nanoprobe was more phototoxic than Ce6 at low concentrations, which was confirmed by flow cytometric assays using the annexin V-FITC/PI apoptotic kit (Fig. 4c). That is, a total of 53.91% apoptotic percentage was obtained for PS@MOF nanoprobe-treated HeLa cells, and only 31.17% for Ce6-treated cells at 0.5 μM (PS equiv.). The real-time monitoring was then performed to evaluate the therapeutic effectiveness (Fig. 4d). The morphology of HeLa cells did not change under irradiation for 12 min in the absence of a photosensitizer. After 3 min irradiation, the PS@MOF nanoprobe-treated HeLa cells began to swell, and more and more bubbles appeared on the surface of cells at a 6 min postirradiation, while the apoptosis characteristics of Ce6-mediated cells occurred after 9 min irradiation, and TMPyP treated-cells did not exhibit any significant morphological change. These results demonstrated that the PS@MOF nanoprobe with low dark toxicity and high phototoxicity could be considered as a potential photosensitizer for highly efficient therapy against cancer.

In summary, an MOF-based multifunctional nanoprobe has been presented for enhancing the $^1O_2$ quantum yield of TMPyP, triggering the photosensitive cell apoptosis and *in situ* monitoring therapeutic efficacy *via* caspase-3 activation. The PS@MOF nanoprobe possesses synthetic convenience, good biocompatibility, high phototoxicity for therapy against cancer cells and excellent specificity to intracellular caspase-3. The high phototoxicity results from the change of the excited level of TMPyP due to its incorporation into the MOF cavity. After FR-mediated uptake, the nanoprobe can efficiently generate $^1O_2$ in mitochondria to induce cell apoptosis with caspase-3 activation, which cleaves the peptide for *in situ* imaging of therapeutic efficacy *via* lighting up the fluorescence of Cy3 labeled to the peptide. At relatively low concentration, its therapeutic efficacy is even superior to conventional Ce6. The unique inner porosity, tunable size, modifiable structure and the sensitization of the MOF endow the theranostic nanoprobe with promising application in precision cancer treatment.

This research was supported by the National Natural Science Foundation of China (21375060, 21135002, 21121091) and Priority development areas of the National Research Foundation for the Doctoral Program of Higher Education of China (20130091130005).

Notes and references

1 N. M. Idris, M. K. Gnanasammandhan, J. Zhang, P. C. Ho, R. Mahendran and Y. Zhang, *Nat. Med.*, 2012, **18**, 1580.
2 M. J. Garland, C. M. Cassidy, D. Woolfson and R. F. Donnelly, *Future Med. Chem.*, 2009, **1**, 667.
3 J. W. Tian, L. Ding, H. X. Ju, Y. Yang, X. Li, Z. Shen, Z. Zhu, J. S. Yu and C. Y. J. Yang, *Angew. Chem., Int. Ed.*, 2014, **53**, 9544.
4 (*a*) P. Horcajada, T. Chalati, C. Serre, B. Gillet, C. Sebrie, T. Baati, J. F. Eubank, D. Heur-taux, P. Clayette and C. Kreuz, *Nat. Mater.*, 2010, **9**, 172; (*b*) C. B. He, K. D. Lu and W. B. Lin, *J. Am. Chem. Soc.*, 2014, **136**, 12253; (*c*) C. B. He, K. D. Lu and W. B. Lin, *J. Am. Chem. Soc.*, 2014, **136**, 5181; (*d*) A. V. Desai, P. Samanta, B. Manna and S. K. Ghosh, *Chem. Commun.*, 2015, **51**, 6111; (*e*) H. T. Zhang, J. W. Zhang, G. Huang, Z. Y. Du and H. L. Jiang, *Chem. Commun.*, 2014, **50**, 12069.
5 (*a*) J. Lee, O. K. Farha, J. Roberts, K. A. Scheidt, S. T. Nguyen and J. T. Hupp, *Chem. Soc. Rev.*, 2009, **38**, 1450; (*b*) M. O'Keeffe and O. M. Yaghi, *Chem. Rev.*, 2012, **112**, 675.
6 (*a*) O. K. Farha, A. M. Shultz, A. A. Sarjeant, S. T. Nguyen and J. T. Hupp, *J. Am. Chem. Soc.*, 2011, **133**, 5652; (*b*) C. Zou, Z. Zhang, X. Xu, Q. Gong, J. Li and C. D. Wu, *J. Am. Chem. Soc.*, 2012, **134**, 87; (*c*) D. W. Feng, Z. Y. Gu, J. R. Li, H. L. Jiang, Z. W. Wei and H. C. Zhou, *Angew. Chem., Int. Ed.*, 2012, **51**, 10307.
7 K. D. Lu, C. B. He and W. B. Lin, *J. Am. Chem. Soc.*, 2014, **136**, 16712.
8 J. F. Lovell, T. W. B. Liu, J. Chen and G. Zheng, *Chem. Rev.*, 2010, **110**, 2839.
9 (*a*) D. J. Ye, A. J. Shuhendler, L. N. Cui, L. Tong, S. S. Tee, G. Tikhomirov, D. W. Felsher and J. H. Rao, *Nat. Chem.*, 2014, **6**, 519; (*b*) J. F. Lovell, M. W. Chan, Q. C. Qi, J. Chen and G. Zheng, *J. Am. Chem. Soc.*, 2011, **133**, 18580; (*c*) Y. Y. Yuan, R. T. K. Kwok, B. Z. Tang and B. Liu, *J. Am. Chem. Soc.*, 2014, **136**, 2546.
10 (*a*) Y. Z. Min, J. M. Li, F. Liu, E. K. L. Yeow and B. G. Xing, *Angew. Chem., Int. Ed.*, 2014, **53**, 1012; (*b*) H. B. Shi, R. T. K. Kwok, J. Z. Liu, B. G. Xing, B. Z. Tang and B. Liu, *J. Am. Chem. Soc.*, 2012, **134**, 17972.
11 K. Stefflova, J. Chen, H. Li and G. Zheng, *Mol. Imaging*, 2006, **5**, 520.
12 J. Park, D. Feng, S. Yuan and H. C. Zhou, *Angew. Chem., Int. Ed.*, 2015, **54**, 430.
13 Z. J. Zhang, L. P. Zhang, L. Wojtas, M. Eddaoudi and M. J. Zaworotko, *J. Am. Chem. Soc.*, 2012, **134**, 928.
14 Q. B. Wang, W. Wang, J. P. Lei, N. Xu, F. L. Gao and H. X. Ju, *Anal. Chem.*, 2013, **85**, 12182.
15 R. W. Larsen, J. Miksovska, R. L. Musselman and L. Wojtas, *J. Phys. Chem.*, 2011, **115**, 11519.
16 S. Chen, A. Osaka, T. Ikoma, H. Morita, J. Li, M. Takeguchi and N. Hanagata, *J. Mater. Chem.*, 2011, **21**, 10942.
17 N. Adarsh, R. R. Avirah and D. Ramaiah, *Org. Lett.*, 2010, **12**, 5720.
18 Z. Zhang and M. J. Zaworotko, *Chem. Soc. Rev.*, 2014, **43**, 5444.
19 X. Zhu, H. Y. Zheng, X. F. Wei, Z. Y. Lin, L. Guo, B. Qiu and G. N. Chen, *Chem. Commun.*, 2013, **49**, 1276.
20 (*a*) S. Nayak, H. Lee, J. Chmielewski and L. A. Lyon, *J. Am. Chem. Soc.*, 2004, **126**, 10258; (*b*) P. Huang, C. Xu, J. Lin, C. Wang, X. Wang, C. Zhang, X. Zhou, S. Guo and D. Cui, *Theranostics*, 2011, **1**, 240.
21 P. M. Kasili, J. M. Song and T. Vo-Dinh, *J. Am. Chem. Soc.*, 2004, **126**, 2799.

